ORIENTAL JOURNAL OF CHEMISTRY
An International Open Access, Peer Reviewed Research Journal
www.orientjchem.org

ISSN: 0970-020 X
CODEN: OJCHEG
2025, Vol. 41, No.(1):
Pg. 01-10

Green Synthesis of Copper Oxide Nanoparticles (CuO-Nps) using *Calotropis procera* Plant Extract: Characterization and Evaluation in the Photocatalytic Degradation of Dye

NOOR AATI ALRISHI[1]*, AMAL MOZAREI IBRAHIM[2], SAEDAH RWEDE ALMHYAWI[3], and ATIKAH MUSA ALNAHARI[4]

[1*]Department of Chemistry, College of Science, University of Jeddah, Jeddah, Saudi Arabia.
[2]Department Advanced Materials Technology and Mineral Resources Research Institute
National Research Center, Cairo, Egypt.
[3,4]Department of Chemistry, College of Science, University of Jeddah, Jeddah, Saudi Arabia.
*Corresponding author E-mail: Noorarishi@outlook.com

http://dx.doi.org/10.13005/ojc/410101

(Received: September 24, 2024; Accepted: January 28, 2025)

ABSTRACT

In recent years, green synthesis has received much attention due to its positive impact on the environment. Copper oxide nanoparticles (CuO-Nps) were synthesized using the co-precipitation method with three different approaches; traditional synthesis (T@CuO-Nps), synthesis via the *Calotropis procera* plant with and without carbon nanotubes (CuO-Nps@*C.procera*@CNT), (CuO-Nps@*C.procera*), respectively. The photocatalytic performance was investigated by removing Alizarine Yellow R (AYR) dye under sunlight. The properties of the CuO-Nps were examined using X-ray diffraction (XRD), scanning electron microscopy (SEM), transmission electron microscopy (TEM), and a Brunauer-Emmett-Teller (BET) analysis. Photocatalytic activities of the CuO-Nps were checked for the removal of AYR dye using a UV-Visible spectrophotometer. It was observed that the removal of dye reached 96.83%, 39.6%, and 32.37% for CuO-Nps@*C.procera*@CNT, CuO-Nps@*C. procera*, and T@CuO-Nps, respectively. Furthermore, the biological activities of the CuO-Nps were tested, and antibacterial efficiency was shown against *Gram+ve* and *Gram-ve* bacterial strains.

Keywords: Photocatalytic, Copper oxide, Carbon nanotubes, *Calotropis procera*, Alizarine yellow R.

INTRODUCTION

Water pollution has become a critical problem that must be studied and resolved in the past few decades. According to the World Water Council, by 2030, the number of people living in water-scare areas will rise to about 3.9 billion[1]. Textile wastewater is one of the most contaminated fluids to be treated because of its high color density[2]. It is high concentrations of toxic organic materials, these contaminations lead to high density of water, changing its salinity, pH, and turbidity[3]. Textile wastewater contains a diverse array of dyes, including anthraquinone dyes, azo dyes, triphenylmethane dyes, nitrogen dyes, phthalocyanine dyes, polymethine dyes, xanthene dyes, and indigoids[4]. Furthermore, it contains inorganic heavy metals, which contribute to the overall contamination[4]. Treatment and eradication of these pollutants are of paramount importance due to their substantial impact on the environment and water quality[5]. The discharge of such contaminated industrial wastewater into the ecosystem causes damage to the natural ecosystem balance. Among the many dyes, Alizarine yellow is one of the most important dyes that affect ecosystems. It is an anionic dye, soluble in water, and is a type of sodium salt azo-dye named 5-[(p-Nitrophenyl) azo] salicylic acid[6]. Alizarine yellow has complex aromatic structures and thus contains long-lasting stability for degradation[6]. Also, it has high toxicity and carcinogenicity and is non-biodegradable in ecosystems; therefore, it must be treated before discharging into the ecosystems[6]. Therefore, finding an effective method to remove these dyes from textile wastewater is essential. Among these several technologies, such as adsorption precipitation, coagulation-flocculation, ozonation, biological methods, and membrane filtration[7–11], have been commonly used for treating dye-laden industrial wastewater. However, these methods are nondestructive, and the contaminants are transferred from one phase to another, which implies that more treatment will be required to eliminate these contaminants. Recently, photocatalysis has emerged as an excellent option for removing organic pollutants from wastewater[12]. Photocatalytic degradation is a promising technology because it has several advantages compared to other processes[13], photocatalysis requires mild conditions and completely decompose organic pollutants with no disposal problems.

In recent years, copper oxide (CuO) has gained much attention since it has good prospects in solar energy cells and environmental purification. CuO is a semiconductor material with a 1.7 eV constructed narrow band gap[14]. Copper oxide nanoparticles (CuO-Nps) have a wide range of applications across different fields, including drug delivery, biomedical application, and antibacterial application[14]. CuO-Nps have been synthesized through many techniques that affect the nano-particles chemical, optical, electrical, and mechanical properties. Consequently, these properties affect the targeted field of applications[15]. On the other hand, carbon nanotubes (CNTs) represent the last century's hub in many fields due to their extraordinary physical, chemical, and electrical properties[16]. There are CNTs were classified into single- and multi-wall (SWCNTs and MWCNTs)[17]. However, the lower cost of MWCNTs motivates research into making an efficient MWCNT-MOx photocatalyst[18]. Different metal oxide/CNTs composites were studied and found to have an improvement in efficiency in the presence of CNTs. Among these metal oxide/CNTs ZnO/CNTs, CuS/CNTs, CuS/CNTs, CuO-SWCNT, and ZnO-SWCNT were prepared and investigated for photocatalyst[19–23]. In general, the physicochemical techniques for synthesizing nanoparticles use hazardous chemicals that generate environmentally unfriendly by-products. Therefore, researchers have become increasingly interested in manufacturing nanoparticles using a green, environmentally friendly approach. *Calotropis procera* is a desert plant referred to as Ushar or Madar in Greco-Arabic medicine[24] (see Fig.1[25]). This plant is a toxic evergreen. It is widely distributed and occurs naturally in different regions of Saudi Arabia[26]. During the past decade, this plant has received more attention, and many studies have been undertaken on each part of it. According to a survey conducted across different regions in the Kingdom of Saudi Arabia, *C. procera* aerial parts and roots are frequently used in traditional medicine to cure a range of illnesses, such as fever, joint discomfort, muscle spasms, and constipation[27]. A previous study reported that flower extracts of *C. procera* can be used as an antibacterial agent against pathogenic organisms[28]. Another report investigated the extract of the leaves of *C. procera* antihyperglycemic activity[29]. In this work, we have now aimed to investigate the synthesis of CuO-Nps via three simple co-precipitation methods to investigate the photocatalytic degradation of Alizarine yellow R (AYR) dye in aqueous solutions under sunlight. Furthermore, the biological activities of the prepared CuO-Nps were examined against pathogenic yeast and *Gram+ve* and *Gram*-ve bacterial strains.

Fig. 1. *Calotropis procera* plant[25]

MATERIAL AND METHODS

Chemicals

The starting materials used in these studies included a 30% ammonium hydroxide solution (NH_4OH), cupric acetate ($Cu(CH_3COO)_2$, 99% pure), dis. H_2O, MWCNTs (95%; 9.5 nm in diameter), and AYR dye. All materials and chemicals were implemented as supplied and provided by Sigma Aldrich Company.

Preparation of *C. procera* plant extract

C. procera plant extract was collected from the garden of Jeddah University, KSA. Healthy plant *C. procera* samples were gathered and rinsed multiple times with water to eliminate dust and contaminants. Then the plant was then sun-dried for six days, ground after drying, and 10 g of plant in the form of powder was then combined with 100 mL of dis. H_2O using a magnetic agitator until the solution was thoroughly mixed. Then, the mixture is placed in the Ultrasonic for 45 minute. Finally, the mix was let cool down until it reached ambient temperature before being filtered through a Whatman filter paper No. 1 for future use in experiments.

Synthesis of T@CuO-Nps

A simple precipitation process was utilized for the preparation of T@CuO-Nps traditionally. For preparation of precursor solutions, is dissolving 10 g of $Cu(CH_3COO)_2$ in 100 mL of dis. H_2O, and stirring at 50°C for 10 minutes. The co-precipitation process was achieved by adding NH_4OH dropwise with continuous stirring to attain the value of the reaction mixture pH at 8. Subsequently, the green-colored precipitate was isolated by centrifugation at 10000 rpm for 10 minutes. The greenish precipitate was then washed multiple times with dis. H_2O to eliminate surface impurities, followed by a rinse with ethyl alcohol to remove any unreacted particles. For one day, the nanoparticles were heated to 100°C in a hot air furnace after thorough multistep washing. Afterward, following a two-hour calcination process at 600°C, with an average temperature rise of 10°C per minute, the powdered green copper hydroxide $Cu(OH)_2$ was pulverized using a mortar made from agate and pestle, sifted, and finally dried. The green color of the precipitate was converted into black-colored copper oxide (CuO) particles during calcination. Moreover, the powder is also used for characterization.

Synthesis of CuO-Nps@*C. procera*

10 g of $Cu(CH_3COO)_2$ dissolved in 100 mL of dis. H_2O and stirred at 50°C for 10 min was the procedure used to synthesize CuO-Nps@ *C. procera*. Then plant extract was added in a 1:1 ratio with the Cu^{2+} solution. The co-precipitation process was achieved by adding NH_4OH dropwise with continuous stirring to attain the pH of the reaction mixture 8. Centrifugation was used at 10000 rpm for ten minutes in order to separate the green-colored precipitate, which was subsequently rinsed multiple times with dis. H_2O and ethanol. Afterward, the obtained precipitate was dried at 100°C overnight. Finally, following a two-hour calcination process at 600°C, with an average temperature rise of 10°C per minute, the powdered green copper hydroxide $Cu(OH)_2$ was pulverized using a mortar made from agate and pestle, sifted, and finally dried. The green color of the precipitate was converted into black-colored copper oxide (CuO) particles during calcination.

Synthesis of CuO-Nps@*C.procera*@CNT

Synthesis of CuO-Nps@*C.procera*@CNT was achieved by dissolving 0.2 g of $Cu(CH_3COO)_2$ in 10 mL of dis. H_2O which contains 0.15 g of MWCNTs. The produced slurry was kept at 50°C for 10 min, with stirring, then the plant extract was added in a 1:1 ratio. The co-precipitation process was achieved by adding NH_4OH dropwise with continuous stirring to attain the value of the reaction mixture pH at 8. The obtained precipitate was separated, washed, and dried as described earlier. The dried green powder was crushed and calcined at 300°C for 2 h in an ambient atmosphere.

Stock solution preparation of AYR dye

One gram of AYR dye powder was dissolved in one liter of dis. H_2O to make a stock solution. The desired concentration of the dye during the photocatalytic process were obtained by dilution of the stock solution. The dye concentration was monitored by UV-Vis spectrophotometer by scanning the absorbance at λ_{max} = range from 200 to 500 nm.

Characterization

XRD was employed to determine the crystallite size and investigate the phase of the nanoparticles that were produced. This method, which employed CuKα radiation and a nickel filter, operating at 40kV and 40mA while scanning in the 2θ range from 20° to 80°. A UV-Visible spectrophotometer (UV-1800 Shimadzu) with a 1 nm resolution was employed to monitor the dye concentration during the photocatalytic process.

The three samples morphology and structure were examined using two distinct microscopy techniques. SEM investigation was performed to assess the surface of the samples. A JEOL JSM-7600F scanning electron microscope was implemented to deliver high-resolution scanning of the sample surfaces in order to achieve this result. The samples internal structure was examined using TEM. Complex images of the samples inner architecture were generated by the JEOL JEM-2100 TEM when it was operating at 200 kV. The TEM was equipped with a CCD camera to enhance the resolution of the images that were acquired. A surface area analysis was performed using Brunauer-Emmett-Teller (BET) methodology, which operates on nitrogen gas adsorption and desorption at a temperature of -196°C (liquid nitrogen). This method yielded substantial data regarding the samples porosity and surface area.

Photocatalytic activity study

Samples were tested for their photocatalytic activity by observing how they degraded AYR dye when exposed to sunlight irradiation. In this experiment, 5g/L of photocatalyst CuO-Nps for the three samples was prepared and AYR dye aqueous solution was added and stirred in the dark for 1 h until equilibrium was reached. After that, the effect of contact time was performed by measuring 25 mg/L dye solution, at different shaking times (60, 120, 180, 240, 300 min) for T@CuO-Nps and CuO-Nps@*C.procera*. Meanwhile, different times were taken at (15, 30, 45, 60, 90, 120, 180, 240, 300 min) for CuO@*C.procera*@CNT, under sunlight. The yellow suspension was transformed into a colorless suspension. Then, the solution was measured after filtration by UV-Vis spectrophotometer.

The removal amount at time t, q_t (mg/g) of the molecule and removal efficiency(%) was calculated by the following equation[30]:

$$q_t = (C_o - C_t) \times V/m \qquad (1)$$

$$\text{Removal efficiency (\%)} = (C_o - C_t)/C_o \times 100\% \qquad (2)$$

In this context, the initial concentration of AYR dye is denoted as C_o (in mg/L). The concentration of the AYR dye at any given time t is represented as C_t (in mg/L). The quantity of adsorbent employed in the experiment is represented by m (in grams). In addition, the volume of the AYR dye solution that is being treated is denoted by V (in liters).

Antibacterial activity

In this experiment, use of the agar well diffusion method was implemented to assess a variety of hazardous species, including pathogenic fungal yeasts, *Gram+ve* and *Gram-ve* bacterial strains. Begin by filling 20 mL of sterile nutritional agar (NA) material into petri plates. A suitable substrate for microbial propagation was provided by the medium after chilling and solidification. Following injection, the pathogenous species were subsequently uniformly distributed across the hardened agar surface. This promoted the dissemination of microorganisms throughout the plate. A sterile instrument was then employed to meticulously create small wells in the agar, each with a radius of 0.9 mm. Each well received 100 µL of the prepared samples. The samples were assessed for their capacity to inhibit microbial growth. After the addition of the samples, the dishes were refrigerated for one hour. This procedure facilitated the diffusion of the materials into the agar, thereby enabling interaction with the microorganisms. Optimal conditions for microbial proliferation were established by incubating the dishes at 37°C for 24 h following the refrigeration process. The zones of inhibition (ZI) surrounding the wells were measured in millimetres after incubation. The efficacy of the samples in suppressing the proliferation of the pathogenic species was demonstrated by the dimensions of these zones[31,32].

RESULTS AND DISCUSSION

X-ray Diffraction Study

X-ray analysis was utilized for crystallite phase determination as well as the crystallite size calculation. Phase and crystallite system determination was achieved by X-ray diffraction study for three samples as shown in Fig. 2. The figure shows a pattern in agreement with (JCPDS-05-0661)[33], with a peak at 2θ = 38.9, 35.7, 48.9 and 61.7 for the T@CuO-Nps sample. In addition, the pattern agrees with (JCPDS-05-0061)[33], and the peaks appeared at 38.9, 35.82, 49, and 61.8 for the CuO-Nps@*C.procera* sample. Meanwhile, the diffractogram assigned for the CuO-Nps@*C.procera*@CNT sample showed a pattern representing CuO-Nps with peaks at 2θ = 35.56, 38.77, 48.29 and 61.57. The figure also showed peaks significatnt to CNTs at 2θ = 23.3 and

26.16. To comprehend the samples properties and potential applications, it is imperative to calculate the average crystallite size. For estimating the size of the crystallite of the synthesized samples, the Scherrer equation was implemented(3);

$$D=K\lambda/\beta \cos\theta \qquad (3)$$

Where, D represents the typical crystallite size. The geometry of the crystallites determines the dimensionless form factor K, which is typically approximately 0.9. Denoted by the symbol λ, the wavelength of the X-ray. β is the FWHM of the peak in the X-ray diffraction pattern, which signifies the peaks expansion as a result of the crystallites finite size. K is the Bragg angle that corresponds to the diffraction peaks position.

The calculated average crystalline size is found to be 41.9, 24.9 and 27 nm for T@CuO-Nps, CuO-Nps@*C.procera*, and CuO-Nps@*C.procera*@ CNT, respectively. Also, the diameter of CNTs was calculated to be ≈3.78 nm.

Morphological analysis

The produced CuO-Nps morphological properties were examined using SEM. Detailed visual information regarding the structure of the surface and nanoparticles morphology is provided by the SEM images of the T@CuO-Nps sample, as illustrated in Fig. 3(a). The image shows an agglomeration of CuO that lacks homogeneity, possibly due to the rapid precipitation process. Fig.3(b) displays the SEM images of the CuO-Nps@C.procera sample, showing agglomeration of CuO with low homogeneity. The SEM images also showed higher porosity of the as-prepared CuO-Nps; these findings may be devoted to the presence of plant extract, which acts as a template for the reaction. Fig.3(c,d) shows the SEM images of the CuO-Nps@C.procera@CNT sample. These showed that CuO-Nps clusters are homogeneously distributed all over the sample

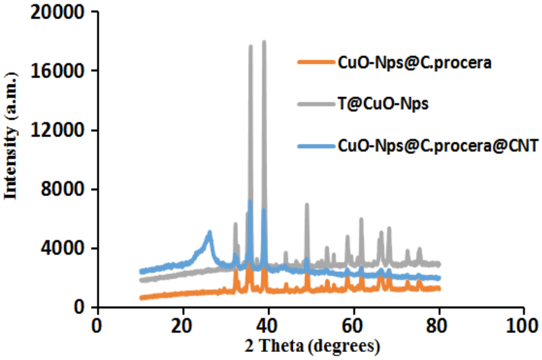

Fig. 2. Comparing the XRD-pattern of the three samples

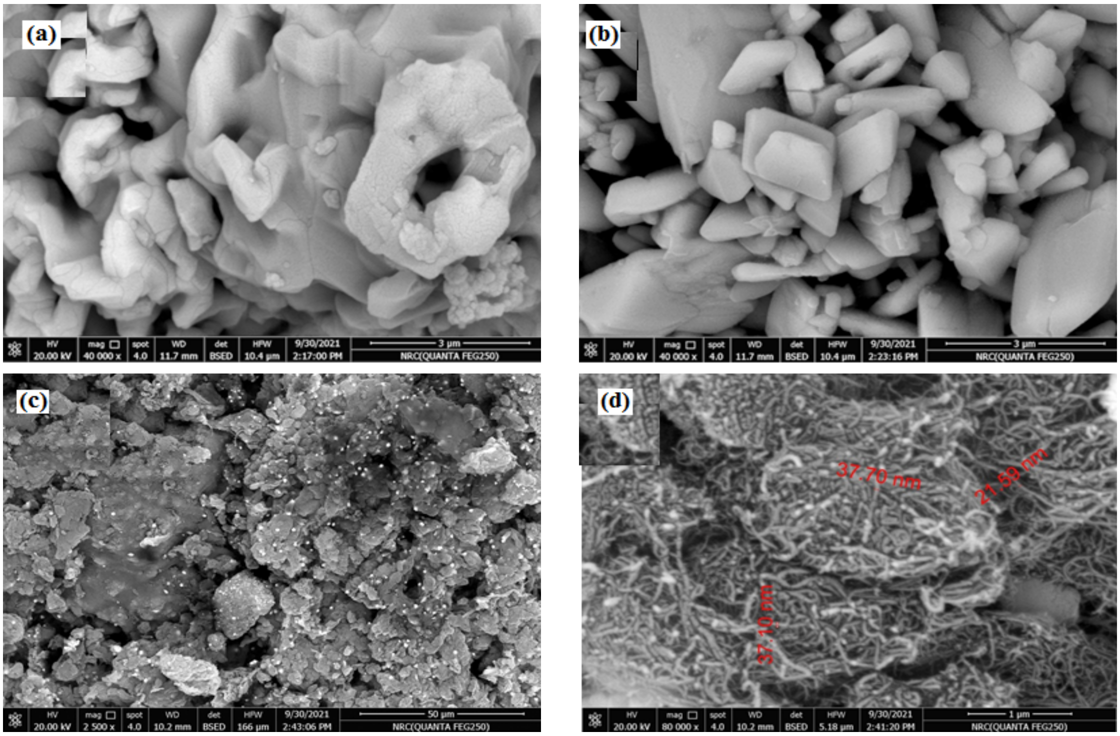

Fig. 3. SEM images of (a) T@CuO-Nps (b) CuO-Nps@*C.procera* (c,d) CuO-Nps@*C.procera*@CNT

The transmission electron microscope study for the sample of CuO-Nps@*C.procera*@CNT is achieved to elucidate the CNTs structure and the nature of CuO-Nps distribution on CNTs. Fig. 4 it is clear from the TEM images that CNTs have a diameter ranging from 3.11 to 13 nm. Most CuO-Nps are deposited outside the CNTs as agglomerates from particles with sizes from 1.9 to 27.5 nm. Only a few CuO-Nps are deposited inside the CNTs.

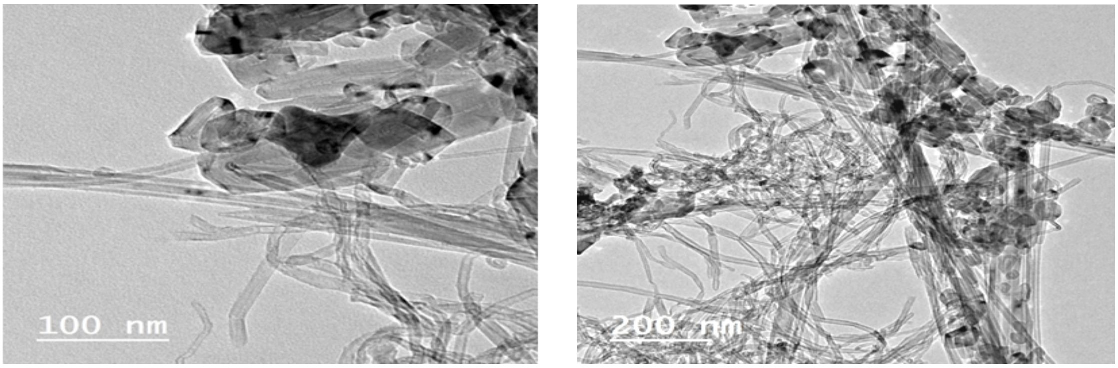

Fig. 4. TEM images of CuO-Nps@*C.procera*@CNT

Brunauer-Emmett-Teller (BET) analysis

The desorption and adsorption of N_2 gas were employed to conduct a surface area investigation at liquid N_2 temperature (-196°C). This approach is helpful in quantifying the samples surface area and pore characteristics, which in turn furnishes critical information regarding its porosity and texture. It was found that the surface area of the prepared samples was 1.835 m^2/g for T@CuO-Nps, and 2.299 m^2/g for CuO-Nps@*C.procera*. Meanwhile, the surface area for CuO-Nps@*C.procera*@CNT was found to be much higher 180.38 m^2/g almost too times higher. The sample of CuO-Nps@*C.procera* has a higher surface area than the T@CuO-Nps sample. This agrees with data from both XRD and SEM which elucidate that green synthesized CuO-Nps has a smaller particle size than the traditionally prepared CuO-Nps.

Adsorption in absence of sunlight irradiation

Firstly, the removal was carried out in a dark place using 25 ppm of AYR dye with adding 0.5g/L of T@CuO-Nps, CuO-Nps@*C.procera*, and CuO-Nps@*C.procera*@CNT. The results, in this case, represent the adsorption process between the solid catalyst and dye solution in the absence of sunlight radiation. It was found, from these experiments, that adsorption efficiency reached equilibrium at 3%, 8.52%, and 37.32% for T@CuO-Nps, CuO-Nps@*C.procera*, and CuO-Nps@*C.procera*@CNT, respectively. Even though the low adsorption efficiency the presence of the CNTs in dye solution largely affects adsorption activity.

Evaluation of CuO-Nps in the removal of AYR dye

The contact time between the dye solution and solid catalyst plays an essential role in removing any environmental pollutants. Hence, a series of experiments were conducted at different contact times of the dye solutions shown in Fig. 5(a,b,c). The findings exhibited an upsurge in the apparent rate constant of the reaction with the increase in the contact time of the solution. Also, it was found, from these experiments, that the efficiency of photocatalysis of the dyes solution for the T@CuO-Nps sample reached 32.37% after 300 min under sunlight as shown in Fig.5(a). Meanwhile, the CuO-Nps@*C.procera* sample reached 39.6% after 300 min under sunlight as shown in Fig.5(b). Furthermore, the efficiency of photocatalytic degradation of dye solution for the CuO-Nps@*C.procera*@CNT sample reached 95.90% within the first 60 min as shown in Fig.5(c). It was found, from these experiments, that the presence of the CNTs affects dramatically the photocatalytic activity in a short time this could be devoted to the increase of the surface area to volume ratio in CNTs. All experiments were performed in triplicate, each being repeated at least three times.

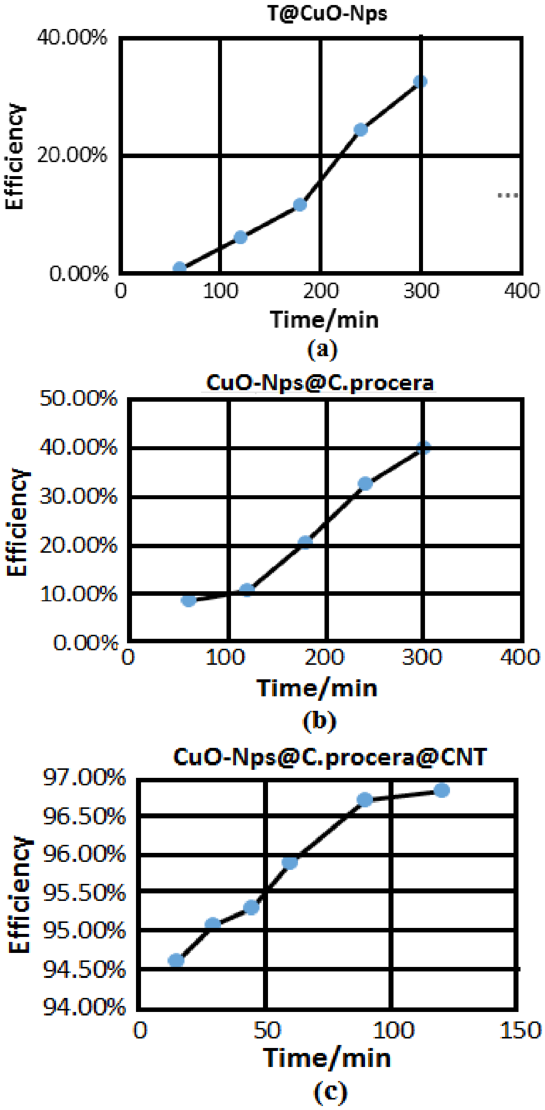

Fig. 5(a,b,c). The effect of contact time on the efficiency of removal of AYR dye from an aqueous solution. The experiments were performed under controlled conditions: AYR dye concentration was established at 25 mg/L, the sample volume was 10 mL, and 0.005 g was utilized. The solution exhibited a pH of 8, with the temperature controlled at 25°C

Antibacterial activity study

The biological activity of CuO-Nps investigated towards both *Gram+ve* and *Gram-ve* bacterial strains in the test samples that were prepared. The T@CuO-Nps sample was found to lack antimicrobial activity, which indicates that it was incapable of damaging the bacterial cell membrane. In contrast, the CuO-Nps@*C.procera* sample revealed antibacterial activity against *S. aureus* and *E. coli*; however, it was ineffective against *P. aeruginosa*, *B. cereus*, and *C. albicans*. Moreover, the CuO-Nps@*C.procera*@CNT sample unveiled antibacterial efficacy against *E. coli, P. aeruginosa*, and *S. aureus*. There are numerous factors that could account for the mechanism of this antibacterial action, including the prohibition of protein biosynthesis, the disruption of the bacterial membrane, the inhibition of nucleic acid synthesis, and the inhibition of cell wall biosynthesis. The eradication of bacterial cells is the result of these actions, which disrupt critical processes within the cells[34]. More specifically, electrostatic forces between bacterial cell membranes and nanoparticles can cause physical harm to the cells, potentially resulting in bacterial death[35]. Also, the small size of nanoparticles facilitates their interaction with bacterial membranes, and bacterial inactivation may occur alongside the penetration of nanoparticles into the bacterial cell[36]. This is supported by XRD and SEM data, which show that green-synthesized CuO nanoparticles have a smaller particle size than traditionally prepared CuO nanoparticles. On the other hand, the three samples T@CuO-Nps, CuO-Nps@*C. procera*, and CuO-Nps@*C.procera*@CNT, have no antimicrobial activity against the pathogenic fungal yeast *C.albicans*, this behavior could be explained by the disability of these samples to injure or destroy the cell membrane, therefore cannot pass inside the cell[37]. The antibacterial activity was assessed by measuring the inhibition zones obtained (Table 1).

Table 1: Diameter of the inhibition zones (in millimetres) for the samples

Samples test bacteria	T@CuO-Nps	CuO-Nps@*C.procera*	CuO-Nps@*C.procera* @CNT	CN*
E. coli	Nil	13	14	17
P. aeruginosa	Nil	Nil	Nil	16
B. cereus	Nil	Nil	12	20
S. aureus	Nil	17	19	25
C. albicans	Nil	Nil	Nil	__

* Nil: No antimicrobial activity recoded

* CN: Gentamycin standard antibiotic disc (10.0 mcg)

CONCLUSION

From this study, it could be concluded clearly that the presence of *C.procera* plant extract in the reaction medium affect greatly the particle size of the prepared CuO-Nps decreasing from 41.9 nm to 24.9 nm for T@CuO-Nps and CuO-Nps@*C.procera*, respectively. Consequently, this decrease in crystallite size affects dramatically the efficiency of CuO-Nps in photocatalytic degradation. Also, it is observed that even though the crystallite size of the CuO-Nps@*C.procera* and CuO-Nps@*C.procera*@CNT samples, the removal efficiency of the CuO-Nps@*C.procera*@CNT sample increases with great extent. This increase is explained by the presence of CNTs which causes an increase in surface area due to the dispersion effect of the CuO-Nps as well as the electromagnetic characteristics of the CNTs which act as co-catalysts and facilitate photocatalytic degradation. Finally, the biological activity studies showed anticipated antibacterial activity which valued the prepared compounds in wastewater treatment.

ACKNOWLEDGEMENT

The authors would like to extend their appreciation to the University of Jeddah for the facilities it provides.

Conflict of interest

The authors declares that they have no conflict of interest.

REFERENCES

1. Xu, J.; Cao, Z.; Zhang, Y.; Yuan, Z.; Lou, Z.; Xu, X.; Wang, X. A Review of Functionalized Carbon Nanotubes and Graphene for Heavy Metal Adsorption from Water: Preparation, Application, and Mechanism., *Chemosphere.,* **2018**, *195*, 351–364. https://doi.org/10.1016/j.chemosphere.2017.12.061.
2. Azanaw, A.; Birlie, B.; Teshome, B.; Jemberie, M. Textile Effluent Treatment Methods and Eco-Friendly Resolution of Textile Wastewater., *Case Studies in Chemical and Environmental Engineering.*, **2022**, *6*, 100230. https://doi.org/https://doi.org/10.1016/j.cscee.2022.100230.
3. Syeed, M. M. M.; Hossain, M. S.; Karim, M. R.; Uddin, M. F.; Hasan, M.; Khan, R. H. Surface Water Quality Profiling Using the Water Quality Index, Pollution Index and Statistical Methods: A Critical Review., *Environmental and Sustainability Indicators.,* **2023**, *18*, 100247. https://doi.org/https://doi.org/10.1016/j.indic.2023.100247.
4. Al-Tohamy, R.; Ali, S. S.; Li, F.; Okasha, K. M.; Mahmoud, Y. A.-G.; Elsamahy, T.; Jiao, H.; Fu, Y.; Sun, J. A Critical Review on the Treatment of Dye-Containing Wastewater: Ecotoxicological and Health Concerns of Textile Dyes and Possible Remediation Approaches for Environmental Safety., *Ecotoxicol Environ Saf.*, **2022**, *231*, 113160. https://doi.org/https://doi.org/10.1016/j.ecoenv.2021.113160.
5. Berradi, M.; Hsissou, R.; Khudhair, M.; Assouag, M.; Cherkaoui, O.; El Bachiri, A.; El Harfi, A., *Textile Finishing Dyes and Their Impact on Aquatic Environs. Heliyon.*, **2019**, *5*(11), e02711.
6. Ahmed, A.; Usman, M.; Yu, B.; Ding, X.; Peng, Q.; Shen, Y.; Cong, H. Efficient Photocatalytic Degradation of Toxic Alizarin Yellow R Dye from Industrial Wastewater Using Biosynthesized Fe Nanoparticle and Study of Factors Affecting the Degradation Rate., *J Photochem Photobiol B.,* **2020**, *202*, 111682. https://doi.org/10.1016/j.jphotobiol.2019.111682.
7. Bazrafshan, E.; Alipour, M. R.; Mahvi, A. H. Textile Wastewater Treatment by Application of Combined Chemical Coagulation, Electrocoagulation, and Adsorption Processes., *Desalination Water Treat.*, **2016**, *57*(20), 9203–9215.
8. Zahrim, A. Y.; Tizaoui, C.; Hilal, N. Coagulation with Polymers for Nanofiltration Pre-Treatment of Highly Concentrated Dyes: A Review., *Desalination.*, **2011**, *266*(1), 1–16. https://doi.org/https://doi.org/10.1016/j.desal.2010.08.012.
9. El Hassani, K.; Kalnina, D.; Turks, M.; Beakou, B. H.; Anouar, A. Enhanced Degradation of an Azo Dye by Catalytic Ozonation over Ni-Containing Layered Double Hydroxide Nanocatalyst., *Sep Purif Technol.*, **2019**, *210*, 764–774. https://doi.org/https://doi.org/10.1016/j.seppur.2018.08.074.

10. Khouni, I.; Marrot, B.; Amar, R. Ben. Treatment of Reconstituted Textile Wastewater Containing a Reactive Dye in an Aerobic Sequencing Batch Reactor Using a Novel Bacterial Consortium., *Sep Purif Technol.,* **2012**, *87*, 110–119. https://doi.org/https://doi.org/10.1016/j.seppur.2011.11.030.
11. Tran, T. T. Van; Kumar, S. R.; Lue, S. J. Separation Mechanisms of Binary Dye Mixtures Using a PVDF Ultrafiltration Membrane: Donnan Effect and Intermolecular Interaction., *J Memb Sci.*, **2019**, *575*, 38–49. https://doi.org/https://doi.org/10.1016/j.memsci.2018.12.070.
12. Mota, A. L. N.; Albuquerque, L. F.; Beltrame, L. T. C.; Chiavone-Filho, O.; Machulek Jr, A.; Nascimento, C. A. O. Advanced Oxidation Processes and Their Application in the Petroleum Industry: A Review. *Brazilian Journal of Petroleum and Gas.*, **2009**, *2*(3).
13. Bhatkhande, D. S.; Pangarkar, V. G.; Beenackers, A. A. C. M. Photocatalytic Degradation for Environmental Applications–a Review., *Journal of Chemical Technology & Biotechnology: International Research in Process, Environmental & Clean Technology.,* **2002**, *77*(1), 102–116.
14. Sathiyavimal, S.; Vasantharaj, S.; Veeramani, V.; Saravanan, M.; Rajalakshmi, G.; Kaliannan, T.; Al-Misned, F. A.; Pugazhendhi, A. Green Chemistry Route of Biosynthesized Copper Oxide Nanoparticles Using Psidium Guajava Leaf Extract and Their Antibacterial Activity and Effective Removal of Industrial Dyes., *J Environ Chem Eng.*, **2021**, *9*(2), 105033. https://doi.org/https://doi.org/10.1016/j.jece.2021.105033.
15. Grigore, M. E.; Biscu, E. R.; Holban, A. M.; Gestal, M. C.; Grumezescu, A. M. Methods of Synthesis, Properties and Biomedical Applications of CuO Nanoparticles., *Pharmaceuticals (Basel).*, **2016**, *9*(4), 75. https://doi.org/10.3390/ph9040075.
16. Anzar, N.; Hasan, R.; Tyagi, M.; Yadav, N.; Narang, J. Carbon Nanotube - A Review on Synthesis, Properties and Plethora of Applications in the Field of Biomedical Science., *Sensors International.*, **2020**, *1*, 100003. https://doi.org/https://doi.org/10.1016/j.sintl.2020.100003.
17. Rümmeli, M. H.; Bachmatiuk, A.; Börrnert, F.; Schäffel, F.; Ibrahim, I.; Cendrowski, K.; Simha-Martynkova, G.; Plachá, D.; Borowiak-Palen, E.; Cuniberti, G.; Büchner, B. Synthesis of Carbon Nanotubes with and without Catalyst Particles., *Nanoscale Res Lett.,* **2011**, *6*(1), 303. https://doi.org/10.1186/1556-276X-6-303.
18. Wang, Y.; Jiang, F.; Chen, J.; Sun, X.; Xian, T.; Yang, H. In Situ Construction of CNT/CuS Hybrids and Their Application in Photodegradation for Removing Organic Dyes., *Nanomaterials.*, **2020**, *10*(1), 178.
19. Kamal Prasad Sapkota, Insup Lee, Md. Abu, Hanif, Md. Akherul Islam, J. R. H. Solar-Light-Driven Efficient ZnO–Single-WalledCarbon Nanotube Photocatalyst for the Degradationof a Persistent Water Pollutant Organic Dye. *Catalysts.,* **2019**, *9*(6).
20. Azqhandi, M. H. A.; Vasheghani F., B.; Rajabi, F. H.; Keramati, M. Synthesis of Cd Doped ZnO/CNT Nanocomposite by Using Microwave Method: Photocatalytic Behavior, Adsorption and Kinetic Study., *Results Phys.*, **2017**, *7*, 1–9. https://doi.org/10.1016/j.rinp.2017.02.033.
21. Bhavyasree, P. G.; Xavier, T. S. Green Synthesis of Copper Oxide/Carbon Nanocomposites Using the Leaf Extract of Adhatoda Vasica Nees, Their Characterization and Antimicrobial Activity., *Heliyon.,* **2020**, *6* (2), e03323.
22. Chen, C. S.; Xie, X. D.; Liu, T. G.; Lin, L. W.; Kuang, J. C.; Xie, X. L.; Lu, L. J.; Cao, S. Y. Multi-Walled Carbon Nanotubes Supported Cu-Doped ZnO Nanoparticles and Their Optical Property., *Journal of Nanoparticle Research.*, **2012**, *14*(4), 817. https://doi.org/10.1007/s11051-012-0817-5.
23. Sorbiun, M.; Shayegan Mehr, E.; Ramazani, A.; Taghavi Fardood, S. Green Synthesis of Zinc Oxide and Copper Oxide Nanoparticles Using Aqueous Extract of Oak Fruit Hull (Jaft) and Comparing Their Photocatalytic Degradation of Basic Violet 3., *Int J Environ Res.*, **2018**, *12*(1), 29–37. https://doi.org/10.1007/s41742-018-0064-4.
24. Mossa, J. S.; Tariq, M.; Mohsin, A.; Ageel, A. M.; Al-Yahya, M. A.; Al-Said, M. S.; Rafatullah, S. Pharmacological Studies on Aerial Parts of Calotropis Procera., *Am J Chin Med (Gard City N Y).*, **1991**, *19*(03n04), 223–231.

25. Habeeb, A.; Ramesh, S.; Shanmugam, R. Calotropis Procera and the Pharmacological Properties of Its Aqueous Leaf Extract: A Review., *Cureus.*, **2024**, *16*. https://doi.org/10.7759/cureus.60354.
26. Hindi, S. *Calotropis Procera: The Miracle Shrub in the Arabian Peninsula.*, **2013**, *2*, 48–57.
27. Al-Yahya, M. A. Saudi Plants: A Phytochemical and Biological Approach; King Abdulaziz City for Science and Technology., **1990**.
28. Ali, A.; Ansari, A.; Qader, S. A. U.; Mumtaz, M.; Saied, S.; Mahboob, T. Antibacterial Potential of Calotropis Procera (Flower) Extract against Various Pathogens., *Pak J Pharm Sci.*, **2014**, *27*, 1565+.
29. Neto, M. C. L.; de Vasconcelos, C. F. B.; Thijan, V. N.; Caldas, G. F. R.; Araújo, A. V; Costa-Silva, J. H.; Amorim, E. L. C.; Ferreira, F.; de Oliveira, A. F. M.; Wanderley, A. G. Evaluation of Antihyperglycaemic Activity of Calotropis Procera Leaves Extract on Streptozotocin-Induced Diabetes in Wistar Rats., *Revista Brasileira de Farmacognosia.,* **2013**, *23* (6), 913–919. https://doi.org/https://doi.org/10.1590/S0102-695X2013000600008.
30. Bishwas, R. K.; Mostofa, S.; Alam, Md. A.; Jahan, S. A. Removal of Malachite Green Dye by Sodium Dodecyl Sulfate Modified Bentonite Clay: Kinetics, Thermodynamics and Isotherm Modeling., *Next Nanotechnology.,* **2023**, *3–4*, 100021. https://doi.org/https://doi.org/10.1016/j.nxnano.2023.100021.
31. Ibrahim, A. M.; Ibrahim, F. A.; Selim, M. Preparation of Non-Stoichiometric Zinc Ferrite/Magnetite [(ZnxFe1- x)O.Fe2O3] Nanoparticles: Adsorption and Biological Activity., *Egypt J Chem.*, **2022**, *65*(131), 185–197. https://doi.org/10.21608/ejchem.2022.135033.5953.
32. Mostafa, H.; Pala, A.; Högel, J.; Hlavac, M.; Dietrich, E.; Westhoff, M. A.; Nonnenmacher, L.; Burster, T.; Georgieff, M.; Wirtz, C. R.; Marion Schneider, E. Immune Phenotypes Predict Survival in Patients with Glioblastoma Multiforme., *J Hematol Oncol.*, **2016**, *9*(1), 1–14. https://doi.org/10.1186/s13045-016-0272-3.
33. Dar, M. A.; Ahsanulhaq, Q.; Kim, Y. S.; Sohn, J. M.; Kim, W. B.; Shin, H. S. Versatile Synthesis of Rectangular Shaped Nanobat-like CuO Nanostructures by Hydrothermal Method; Structural Properties and Growth Mechanism., *Appl Surf Sci.*, **2009**, *255* (12), 6279–6284. https://doi.org/https://doi.org/10.1016/j.apsusc.2009.02.002.
34. Mc Dermott, P. F.; Walker, R. D.; White, D. G. Antimicrobials: Modes of Action and Mechanisms of Resistance., *Int J Toxicol.,* **2003**, *22*(2), 135–143.
35. Dwivedi, S.; Wahab, R.; Khan, F.; Mishra, Y. K.; Musarrat, J.; Al-Khedhairy, A. A. Reactive Oxygen Species Mediated Bacterial Biofilm Inhibition via Zinc Oxide Nanoparticles and Their Statistical Determination., *PLoS One.,* **2014**, *9*(11), e111289.
36. Vardanyan, Z.; Gevorkyan, V.; Ananyan, M.; Vardapetyan, H.; Trchounian, A. Effects of Various Heavy Metal Nanoparticles on Enterococcus Hirae and Escherichia Coli Growth and Proton-Coupled Membrane Transport., *J Nanobiotechnology.*, **2015**, *13*, 1–9.
37. Kim, K.-J.; Sung, W. S.; Suh, B. K.; Moon, S.-K.; Choi, J.-S.; Kim, J. G.; Lee, D. G. Antifungal Activity and Mode of Action of Silver Nano-Particles on Candida Albicans., *Biometals.,* **2009**, *22*(2), 235–242.